CHEMISTRY OF MATERIALS

COMMUNICATION

pubs.acs.org/cm

Room-Temperature Synthesis of ZIF-8: The Coexistence of ZnO Nanoneedles

Minqi Zhu,[†] Surendar R. Venna,[†,‡] Jacek B. Jasinski,[§] and Moises A. Carreon*[,†]

[†]Department of Chemical Engineering and [§]Conn Center for Renewable Energy Research, University of Louisville, Louisville, Kentucky 40292

Supporting Information

KEYWORDS: Zeolite imidazolate frameworks, ZnO nanoneedles, kinetics of transformation

Zeolite imidazolate frameworks (ZIFs) are novel type of microporous crystalline materials displaying unique and highly desirable properties from both zeolites and metal organic frameworks, such as remarkable high surface areas, crystallinity, unimodal micropores, as well as thermal and chemical stability.[1] Typically, ZIFs are composed of Zn and Co atoms linked through N atoms by ditopic imidazolate (Im) or functionalized Im links to form neutral frameworks and to provide tunable nanosized pores formed by four-, six-, eight-, and twelve-membered ring ZnN_4, and CoN_4 tetrahedras.[1b] Although the great potential of ZIFs as novel functional materials has been demonstrated recently in diverse fields, including gas separations,[2] sensing,[3] and catalysis,[4] to the best of our knowledge, only few reports,[5] including our recent work,[5a] has been published on the mechanistic aspects of ZIFs formation. A basic understanding on the formation mechanisms of zeolitic imidazolate frameworks is important to rationally develop materials with tailored structural, compositional, and morphological properties. Herein, we followed the crystallization-time dependence of a representative zeolitic imidazolate framework, ZIF-8 which has large pores of 11.6 Å accessible through small apertures of 3.4 Å.[6] Interestingly, when zinc carbonate basic was used as the metal source, the coexistance of ZIF-8 and ZnO nanoneedles was observed.

ZIF-8 crystals were prepared as follows: 2.8 mmol of zinc carbonate basic ($[ZnCO_3]_2 \cdot [Zn(OH)_2]_3$, Sigma Aldrich) were dissolved in 1.4 mol of methanol (Acros Organics, extra dry, water <50 ppm). A solution consisting of 64.4 mmol of 2-methylimidazole ($C_4H_6N_2$, Aldrich, 99%) and 1.4 mol of methanol was added to the Zn based solution and vigorously stirred for different times. Finally, this solution was centrifugated at 3000 rpm, and washed thoroughly with methanol. This procedure was repeated 3 times. The resultant crystals were dried overnight at 120 °C. Powder X-ray diffraction patterns were collected using a Bruker D8-Discover diffractometer at 40 kV, 40 mA with Cu Kα radiation. Transmission electron microscopy (TEM) studies, including TEM imaging, selected area electron diffraction (SAED), and energy-dispersive X-ray spectroscopy (EDS), were performed using a FEI Tecnai F20 transmission electron microscope. A field emission gun (FEG) was used for the electron source and the studies were performed at the accelerating voltage of 200 keV. Samples for TEM analysis were prepared by dispersing the powders onto lacey-carbon coated copper TEM grids. ZIF-8 is highly sensitive to the electron beam damage. Therefore, low-dose imaging and diffraction conditions (highly diverged beam with increased spot size corresponding to low beam current density) were employed. In order to obtain the analytical information from individual nanoparticles, the EDS analysis was performed in the nanoprobe mode and the beam diameter of 1 nm was selected. The surface area and adsorption−desorption isotherm measurements were carried out on Micromeritics Tristar 3000 porosimeter at 77 K using liquid nitrogen as coolant and the samples were degassed at 150 °C for 3 h before the measurements.

Figure 1 shows the XRD patterns of the ZIF-8 samples synthesized in the presence of zinc carbonate basic at different synthesis times. Reflections of higher order for ZIF-8 corresponding to the planes (011), (022), (112), (022), (013), and (222) increased as time progressed. The area under the curve of all these peaks was quantified using origin software, after baseline correction, to determine the relative crystallinity curve of ZIF-8 phase (see Figures S1−S6 and Table S1 in the Supporting Information). This curve can be directly related to the phase transformation rate. As shown in Figure 1, the presence of defined XRD peaks at 10 min indicates that ZIF-8 forms even at this short synthesis time. Below 10 min, there is an induction period required to nucleate the ZIF-8 phase.

Figure 2 shows the crystallization rate curve of ZIF-8 and the data points represent the total measured intensity of the six primary XRD reflections of ZIF-8. Individual analysis for each reflection is shown elsewhere.[7] The relative crystallinity of ZIF-8 increased linearly during the first 2 h from ∼20 to ∼40%. Then the rate of crystallization increased slowly from 2 to 24 h from ∼40 to ∼60%. Finally, after 48 h the relative crystallinity of ZIF-8 remained ∼80%, reaching a maximum of 100% at 120 h.

The specific BET surface areas of all samples correlated with the ZIF-8 relative crystallinity (Figure 2). For example, surface areas increased linearly at short synthesis times and remained practically constant in the 48−120 h range. It is important to mention that the apparent surface area was evaluated using the BET method and taking the data in the $0.01 < P/P_0 < 0.3$ range. The relatively low observed surface areas may indicate that the synthesized ZIF-8 still contains some unreacted 2-methylimidazole linker that was not desorbed from the framework. Interestingly, in the growth regime, the kinetics of transformation followed Avrami's model[8] (inset of Figure 2). Therefore, the relative crystallinity of ZIF-8 as a function of time in this region can be

Received: June 15, 2011
Revised: July 24, 2011
Published: July 29, 2011

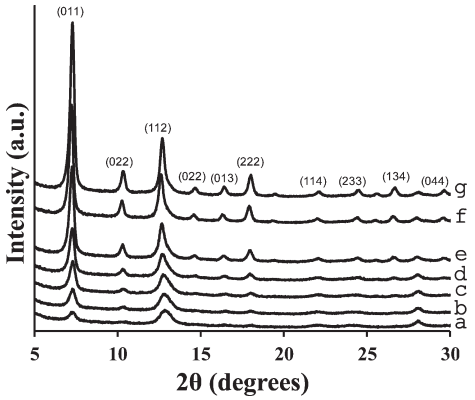

Figure 1. XRD patterns of ZIF-8 as a function of synthesis time: (a) 10 min; (b) 30 min; (c) 2 h; (d) 6 h; (e) 24 h; (f) 48 h; and (g) 120 h.

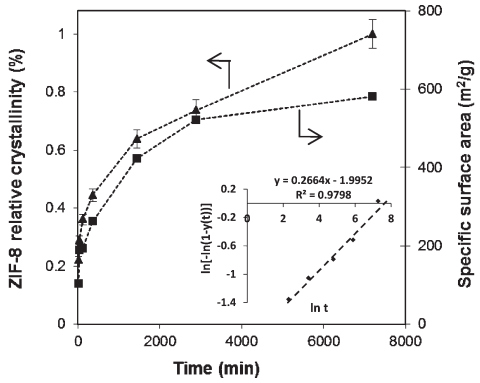

Figure 2. Crystallization rate curve of ZIF-8 and its correlation with specific surface area. Inset shows that the growth regime follows Avrami's kinetics.

expressed as $y = 1 - \exp[-kt^n]$, where k is a scaling constant, and n is the Avrami's constant. For our case, $k = 0.14$, and $n \approx 0.27$. Although typical values of Avrami's n constant are in the 1−4 range, this constant can adopt different values, including fractional numbers below 1.[9a] Values of the Avrami exponent below 1 have been typically attributed to both decreasing nucleation and growth rates as crystallization proceeds.[9a] Values of Avrami's constant of 0.2 and 0.3 have been observed for some alloys.[9a−c]

Figure 3 shows TEM images of selected samples synthesized at different synthesis times. Interestingly, the presence of a second phase in nanoneedle form was observed for samples synthesized from 10 min to 48 h. At 30 min, ∼30 nm ZIF-8 crystallites, some of them already faceted coexist with nanoneedles displaying ∼10−20 nm diameter and lengths in the ∼100−150 nm range (Figure 3a,b). As time progressed, the size of the ZIF-8 crystals increased to ∼50−60 nm, with no evident size growth of the nanoneedle-like phase (Figure 3c,d). Finally, at 120 h, only well-faceted ∼80−90 nm hexagonal and cubic-like crystals corresponding to pure ZIF-8 phase were observed (Figure 3e,f). It is important to mention that only for the sample synthesized at 120 h, pure ZIF-8 crystals were present (no nanoneedles), suggesting that at this time the complete crystallization of the microporous framework takes place. The TEM images revealed that increasing the crystallization time led to an increase in crystal ZIF-8 crystal size due to Ostwald ripening, a well-known thermodynamically driven process, in which small crystals disappear at the expense of the formation of larger crystals. The disappearance of the nanoneedles at long synthesis

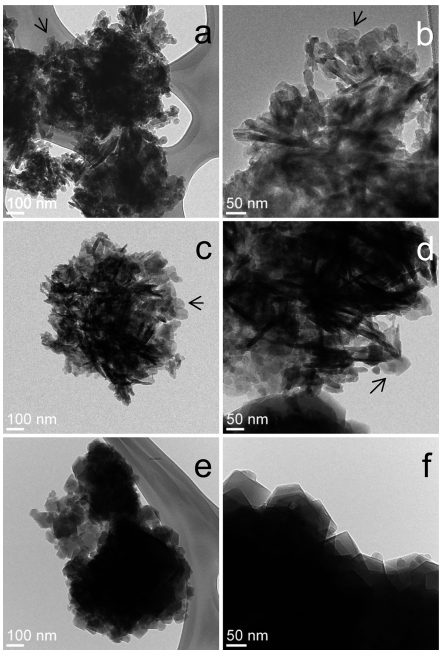

Figure 3. Representative TEM images of ZIF-8 as a function of synthesis time: (a,b) 30 min; (c, d) 24 h; (e, f) 120 h. In a−d, arrows indicate ZIF-8 phase. e and f are pure ZIF-8 crystals.

times indicate that this is a metastable phase that coexists with ZIF-8 at low (10 min) to moderate (48 h) synthesis times.

SAED and EDS study were carried out to identify the composition and crystal structure of the nanoneedles. A typical SAED ring pattern obtained from a sample with high density of nanoneedles is shown in Figure 4a. The radial intensity distribution profile, measured from this pattern is plotted in Figure 4b (black line). It agrees with a database XRD pattern of wurtzite ZnO (JCPDS pattern 01−075−0576), and the SAED rings at d-spacing of 0.356, 0.405, 0.524, 0.617, 0.678, 0.727, 0.738, and 0.917 nm correspond to the reflection from: (100), (101), (102), (110), (103), (112), (201), and (202) crystal planes, respectively. The TEM image shown in Figure 4c shows nanoneedles with ∼20 nm diameter and lengths in the ∼100−200 nm range. The SAED pattern and the radial intensity distribution profile are in agreement with the EDS measurements, which confirms that nanoneedles are composed of zinc and oxygen, as shown in Figure 4d, where an EDS spectrum obtained from a single nanoneedle is presented. Elemental quantification of this spectrum yields 49 ± 2 and 51 ± 2 at % of Zn and O, respectively, which is in excellent agreement with ZnO. In addition to ZnO rings, the SAED pattern consists of three additional rings at the d-spacing of 0.312, 0.268, and 0.155 nm, respectively. The origin of these rings it is not clear.

It is important to mention that ZnO nanoneedles were only observed when Zn carbonate basic was used as the metal source. Other zinc precursors including Zn sulfate, Zn nitrate and Zn chloride led only to hexagonal and cubic faceted crystals, typical morphology of pure ZIF-8 phase.[7] Different from sulfate, nitrate and chloride counterions, the presence of carbonate basic in the synthesis gel leads to a rich hydroxyl species solution environment. It is likely then that the dehydration of these hydroxyl species results in the formation of ZnO nuclei. At this point, the ZnO nanoneedles can grow by condensation of these hydroxyl species.[10] The nanorod-like or nanoneedle-like morphology has been observed when organic amino groups are present as

dx.doi.org/10.1021/cm201701f |*Chem. Mater.* 2011, 23, 3590–3592

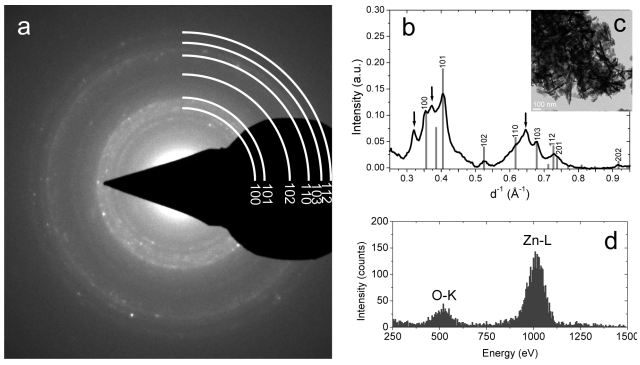

Figure 4. (a) SAED pattern and (b) its radial intensity profile measured for a sample containing high concentration of nanoneedles. Diffraction rings corresponding to wurtzite ZnO are indexed. (c) TEM image of ZnO nanoneedles. (d) EDS spectrum measured from one of such nanoneedles (sample synthesized for 2 h).

additives in the synthesis gel. For instance, zinc oxide nanorods have been synthesized in the presence of ethylenediamine,[11a,9b] triethanolamine,[11b] diethylenetriamine11c,d and hexamethylenetetramine.[11c,e,f] In our case, part of the 2-methylimidazole coordinates with Zn to form ZIF-8, while the unreacted 2-methylimidazole (which is in excess in our prevailing synthesis conditions) may act as the organic amino group catalyst promoting the formation of ZnO nanoneedles. It has been proposed that diverse amino group functionalities with Lewis basic character, can play multiple roles in the formation of ZnO nanorods, including the effective control of the precipitation and passivation of crystal surfaces.[10b,11g] In general, the formation of rod/wire-like ZnO morphologies is promoted at basic pH.[10b] Basic conditions are crucial because metal ions do not readily hydrolyze in acidic media.[11h] The prevailing pH conditions (9.7 < pH < 10) in our synthesis may favor the formation of nanoneedle-like morphologies.

Summarizing, we have studied the formation of ZIF-8 as a function of time at room temperature employing zinc carbonate basic as the metal source. We have found that at short to moderate synthesis times, ZIF-8 crystals and ZnO nanoneedles coexist. Long synthesis times promoted the complete crystallization of ZIF-8. Different from other counterions, the presence of carbonate basic in the synthesis gel led to a rich hydroxyl species solution environment. The condensation of these hydroxyl species resulted in the formation of ZnO nanoneedles. In addition, we demonstrate that the kinetics of transformation of ZIF-8 is governed by Avrami's classic model. A basic understanding on the formation mechanisms of zeolitic imidazolate frameworks presented here is relevant and important to rationally develop metal organic frameworks with tailored properties.

■ ASSOCIATED CONTENT

Ⓢ Supporting Information. Calculation of ZIF-8 relative crystallinity, specific surface area as a function of synthesis time, and XRD/TEM images of ZIF-8 synthesized with zinc nitrate hexahydrate, zinc sulfate monohydrate, and zinc chloride. This material is available free of charge via the Internet at http://pubs.acs.org/

■ AUTHOR INFORMATION

Corresponding Author

*E-mail: macarr15@louisville.edu.

Present Addresses

‡School of Chemical and Biological Engineering, Georgia Institute of Technology, Atlanta, GA 30332.

■ ACKNOWLEDGMENT

This work was supported by NSF CAREER award (CBET#1054150). We thank Gregor Filipic for the development of the software used to obtain the diffraction pattern intensity profile.

■ REFERENCES

(1) (a) Hayashi, H.; Côte, A. P.; Furukawa, H.; O'Keeffe, M.; Yaghi, O. M. *Nat. Mater.* **2007**, *6*, 501. (b) Banerjee, R.; Phan, A.; Wang, B.; Knobler, C.; Furukawa, H.; O'Keeffe, M. *Science* **2008**, *319*, 939. (c) Wang, B; Côte, A. P.; Furukawa, H.; O'Keeffe, M.; Yaghi, O. M. *Nature* **2008**, *453*, 207. (d) Morris, W.; Doonan, C. J.; Furukawa, H.; Banerjee, R.; Yaghi, O. M. *J. Am. Chem. Soc.* **2008**, *130*, 12626. (e) Banerjee, R.; Furukawa, H.; Britt, D.; Knobler, C.; O'Keeffe, M.; Yaghi, O. M. *J. Am. Chem. Soc.* **2009**, *131*, 3875. (f) Phan, A.; Doonan, C. J.; Uribe-Romo, F. J.; Knobler, C. B.; O'Keeffe, M.; Yaghi, O. M. *Acc. Chem. Res.* **2010**, *43*, 58.

(2) (a) Venna, S. R.; Carreon, M. A. *J. Am. Chem. Soc.* **2010**, *132*, 76. (b) Bux, H.; Liang, F.; Li, Y.; Cravillon, J.; Wiebcke, M.; Caro, J. *J. Am. Chem. Soc.* **2009**, *131*, 16000. (c) Liu, Y.; Hu, E.; Khan, E. A.; Lai, Z. *J. Membr. Sci.* **2010**, *353*, 36. (d) Huang, A.; Bux, H.; Steinbach, F.; Caro, J. *Angew. Chem., Int. Ed.* **2010**, *49*, 4958. (e) Li, Y.; Liang, F.; Bux, H.; Yang, W.; Caro, J. *J. Membr. Sci.* **2010**, *354*, 48. (f) Li, Y.; Bux, H.; Feldhoff, A.; Li, G.; Yang, W.; Caro, J. *Adv. Mater.* **2010**, *22*, 3322. (g) McCarthy, M. C.; Varela-Guerrero, V.; Barnett, G. V.; Jeong, H.-K. *Langmuir* **2010**, *26*, 14636. (h) Huang, A.; Caro, J. *Angew. Chem., Int. Ed.* **2011**, *50*, 4979. (i) Bux, H.; Feldhoff, A.; Cravillon, J.; Wiebcke, M.; Li, Y.-S.; Caro, J. *Chem. Mater.* **2011**, *23*, 2262.

(3) (a) Lu, G.; Hupp, J. T. *J. Am. Chem. Soc.* **2010**, *132*, 7832. (b) Liu, S.; Xiang, Z.; Hu, Z.; Zheng, X.; Cao, D. *J. Mater. Chem.* **2011**, *21*, 6649.

(4) (a) Jiang, H. L.; Liu, B.; Akita, T.; Haruta, M.; Sakurai, H.; Xu, Q. *J. Am. Chem. Soc.* **2009**, *131*, 11302. (b) Chizallet, C.; Lazare, S.; Bazer-Bachi, D.; Bonnier, F.; Lecocq, V.; Soyer, E.; Quoineaud, A.; Bats, N. *J. Am. Chem. Soc.* **2010**, *132*, 12365. (c) Tran, U. P. N.; Le, K. K. A.; Phan, N. T. S. *ACS Catal.* **2011**, *1*, 120.

(5) (a) Venna, S. R.; Jasinski, J. B.; Carreon, M. A. *J. Am. Chem. Soc.* **2010**, *132*, 18030. (b) Cravillon, J.; Nayuk, R.; Springer, S.; Feldhoff, A.; Huber, K.; Wiebcke, M. *Chem. Mater.* **2011**, *23*, 2130.

(6) (a) Huang, X.-C.; Lin, Y.-Y.; Zhang, J.-P.; Chen, X-M *Angew. Chem., Int. Ed.* **2006**, *45*, 1557. (b) Park, K. S.; Ni, Z.; Cote, A. P.; Choi, J. Y.; Huang, R.; Uribe-Romo, F. J.; Chae, H. K.; O'Keeffe, M.; Yaghi, O. M. *Proc. Natl. Acad. Sci. U.S.A.* **2006**, *103*, 10186. (c) Cravillon, J.; Muzer, S.; Lohmeier, S. J.; Feldhoff, A.; Huber, K.; Wiebcke, M. *Chem. Mater.* **2009**, *21*, 1410.

(7) See the Supporting Information

(8) (a) Avrami, M. *J. Chem. Phys.* **1939**, *7*, 1103. (b) Avrami, M. *J. Chem. Phys.* **1940**, *8*, 212. (c) Avrami, M. *J. Chem. Phys.* **1941**, *9*, 177.

(9) (a) Pradell, T.; Crespo, D.; Clavaguera, N.; Clavaguera-Mora, M. Y. *J. Phys.: Condens. Matter* **1998**, *10*, 3833. (b) Hampel, G.; Pundt, A.; Hesse, J. *J. Phys.: Condens. Matter* **1992**, *4*, 3195. (c) Cserei, A.; Jiang, J.; Aubertin, F.; Gonser, U. *J. Mater. Sci.* **1994**, *29*, 1213.

(10) (a) Yamabi, S.; Imai, H. *J. Mater. Chem.* **2002**, *12*, 3773. (b) Greene, L. E.; Yuhas, B. D.; Law, M.; Zitoun, D.; Yang, P. *Inorg. Chem.* **2006**, *45*, 7535.

(11) (a) O'Brien, P.; Saeed, T.; Knowles, J. *J. Mater. Chem.* **1996**, *6*, 1135. (b) Trindade, T.; Dejesus, J. D. P.; O'Brien, P. *J. Mater. Chem.* **1994**, *4*, 1611. (c) Greene, L. E.; Law, M.; Goldberger, J.; Kim, F.; Johnson, J. C.; Zhang, Y. F.; Saykally, R. J.; Yang, P. D. *Angew. Chem.. Int. Ed.* **2003**, *42*, 3031. (d) Zhang, H.; Yang, D. R.; Ma, X. Y.; Que, D. L. *J. Phys. Chem. B* **2005**, *109*, 17055. (e) Vayssieres, L.; Keis, K.; Lindquist, S. E.; Hagfeldt, A. *J. Phys. Chem. B.* **2001**, *105*, 3350. (f) Vayssieres, L. *Adv. Mater.* **2003**, *15*, 464. (g) Li, Y.; Tan, B.; Wu, Y. *Chem. Mater.* **2008**, *20*, 567. (h) Verges, M. A.; Mifsud, A.; Serna, C. J. *J. Chem. Soc., Faraday Trans.* **1990**, *86*, 959.